Available online at www.sciencedirect.com
ScienceDirect
Journal of the European Ceramic Society 27 (2007) 1001–1016
www.elsevier.com/locate/jeurceramsoc

A comparative study of the influence of milling media on the structural and microstructural changes in monoclinic ZrO_2

G. Štefanić *, S. Musić, A. Gajović

Ruđer Bošković Institute, Bijenička c. 54, P.O. Box 180, HR-10002 Zagreb, Croatia

Available online 23 June 2006

Abstract

Structural and microstructural developments of *m*-ZrO_2 during the ball-milling process strongly depend on the type of milling assembly used. Ball-milling with corundum milling assembly cause almost complete amorphization of the starting *m*-ZrO_2, while ball-milling with agate or stainless steel assembly cause a decrease of the volume-averaged domain size up to ∼9 nm or ∼13 nm, respectively. Regardless of the type of milling assembly, a small amount of *t*-ZrO_2 appeared in the milled products. The onset of *m*-ZrO_2 → *t*-ZrO_2 transition occurred only in products ball-milled with stainless steel assembly and resulted in a complete transition after 20 h and probable further transition into *c*-ZrO_2 after prolonged milling. The stabilization of *t*- and *c*-ZrO_2 in this products resulted from the incorporation of aliovalent cations due to the wear and oxidation of the milling media. The small fraction of *t*-ZrO_2 in the product milled with corundum or agate milling assembly could not be clearly connected with the effect of crystallite size decrease.

Keywords: Milling; Electron microscopy; X-ray methods; ZrO_2; Rietveld

1. Introduction

According to temperature, ZrO_2 appears in three different polymorphs: monoclinic (*m*-), tetragonal (*t*-) and cubic (*c*-) of which only *m*-ZrO_2 is thermodynamically stable at RT. The reason(s) for the appearance of high-temperature *t*-ZrO_2 at RT has been investigated intensively. There are several proposed models that emphasize the stabilizing influence of the crystallite size,[1,2] lattice strains,[3] anionic impurities,[4] structural similarities between the starting material and *t*-ZrO_2 product,[5] lattice defects (oxygen vacancies),[6,7] etc. A critical review of the subject has been prepared by Štefanić and Musić.[8]

The first report on partial-phase transition from *m*-ZrO_2 to *t*-ZrO_2 caused by ball-milling was given by Bailey et al.[9] The formation of a high-temperature polymorph of ZrO_2 was attributed to the surface energy effect in accordance with the model proposed by Garvie.[1,2] The authors also noticed that the presence of impurities significantly influences the stability of *t*-ZrO_2 product. However, most of the following investigations[10–14] neglected the effect of impurities. Murase and Kato[15] examined the *t*-ZrO_2 → *m*-ZrO_2 transition during the ball-milling at different atmospheres and found that the absence of oxygen or water significantly increased the stability of metastable *t*-ZrO_2.

Our recent investigation showed that a significant decrease of the *m*-ZrO_2 crystallites (below 10 nm) has little or no influence on the *m*-ZrO_2 → *t*-ZrO_2 transition when the ZrO_2 milling assembly, which reduces the influence of an additional material, is used.[16] It was concluded that the impurities introduced due to the wearing of the milling medium are probably more responsible for the stabilization of tetragonal ZrO_2 polymorph, observed in earlier ball-milling experiments, than the particle size (surface energy effect). A small possibility of direct *m*-ZrO_2 → *c*-ZrO_2 transition could not be completely discounted, because a small amount of *c*-ZrO_2 was present in the samples due to the wearing of the milling medium.[16] However, such a transition without an intermediate appearance of *t*-ZrO_2 phase is highly unlikely.

Recently, two papers reported a direct *m*-ZrO_2 → *c*-ZrO_2 transition without any additives, caused by ball-milling with stainless steal milling assembly.[17,18] Both investigations based their conclusions upon the results of diffraction analysis of very small crystallites.

In the present research, the results of X-ray powder diffraction phase analysis were combined with the results of Raman spectroscopy, which proved to be the most powerful technique in cases where the presence of a tetragonal or cubic polymorph of ZrO_2 could not be clearly distinguished using diffraction anal-

* Corresponding author. Tel.: +385 1 456 1111; fax: +385 1 468 0084.
E-mail address: stefanic@irb.hr (G. Štefanić).

0955-2219/$ – see front matter © 2006 Elsevier Ltd. All rights reserved.
doi:10.1016/j.jeurceramsoc.2006.04.136

ysis alone.[19–21] The aim of the investigation was to examine the influence of milling medium (corundum, agate, stainless steel) on the structural and microstructural changes in *m*-ZrO_2.

2. Experimental

The starting material was a monoclinic ZrO_2, Puratronic®, 99.978% (metal basis), produced by Alfa Aesar. Milling with Fritsch planetary ball mill "Pulverisette 6" was performed in air using sintered corundum (99.7% α-Al_2O_3, $\rho = 3.7\ g\ cm^{-3}$), agate (99.9% α-SiO_2, $\rho = 2.65\ g\ cm^{-3}$) and stainless steel (74% Fe + 18% Cr + 8% Ni, $\rho = 7.9\ g\ cm^{-3}$) milling assemblies (grinding balls, $d = 10$ mm, and 80 ml grinding bowls). The rotation speed was 500 rpm and the powder-to-ball weight ratios 1:10. Milling time varied from 10 min to more than 30 h.

Structural and microstructural changes in the ball-milled products were investigated at RT using X-ray powder diffraction, Raman spectroscopy, ^{57}Fe Mössbauer spectroscopy, field emission scanning electron microscopy (FE SEM) and energy dispersive X-ray spectrometry (EDS).

XRD measurements were performed using a Philips counter diffractometer MPD1880 with monochromatized Cu*K*α radiation (graphite monochromator). Silicon, α-Si (space group $m\bar{3}m$, $a = 5.43088$ Å)[22] was used as a standard for the approximation of instrumental profile and a precise determination of lattice parameters.

Raman spectra were recorded using a computerized DILOR Z24 triple monochromator with Coherent INNOVA 100 argon ion laser, operating at 514.5 and 488 nm line for excitation. An Anaspec's doublepass prism premonochromator was used to reduce parasite laser plasma lines. Laser power of 60 mW was applied. To reduce the heating of the samples during recording of the spectra, the incident beam was focused in the line shape.

Mössbauer spectra were recorded in the transmission mode using a spectrometer manufactured by Wissenschaftliche Elektronik GmbH (Starnberg, Germany). ^{57}Co in a rhodium matrix was used as the Mössbauer source. The spectrometer was calibrated with α-Fe. Mössbauer spectra were fitted using the MOSSWINN program.

FE SEM/EDS analyses of uncoated samples were made using the field emission scanning electron microscope JSM-7000F (JEOL) equipped with an energy dispersive X-ray spectrometer INCA/350 EDS Microanalysis System (Oxford Instruments).

3. Powder-pattern fitting methods

The crystallite size and micro-strain of the ball-milled *m*-ZrO_2 products were estimated from the results of whole-powder-pattern profile refinements (program GSAS[23]) following the procedure proposed in the Size/Strain Round Robin.[24] Due to the presence of contaminations and amorphous phase, the refinements were performed using Le Bail method (refinement without structural constraints[25]). XRD patterns were scanned in 0.05° steps (2θ), in the 2θ range from 20° to 80°. In the refinement we used a modified pseudo-Voigt function defined by Thompson, Cox and Hastings,[26] which gave the following expression for Gaussian and Lorentzian observed line widths:

$$\Gamma_G^2 = U\ \tan^2\ \theta + V\ \tan\ \theta + W + \frac{P}{\cos^2\ \theta} \quad (1)$$

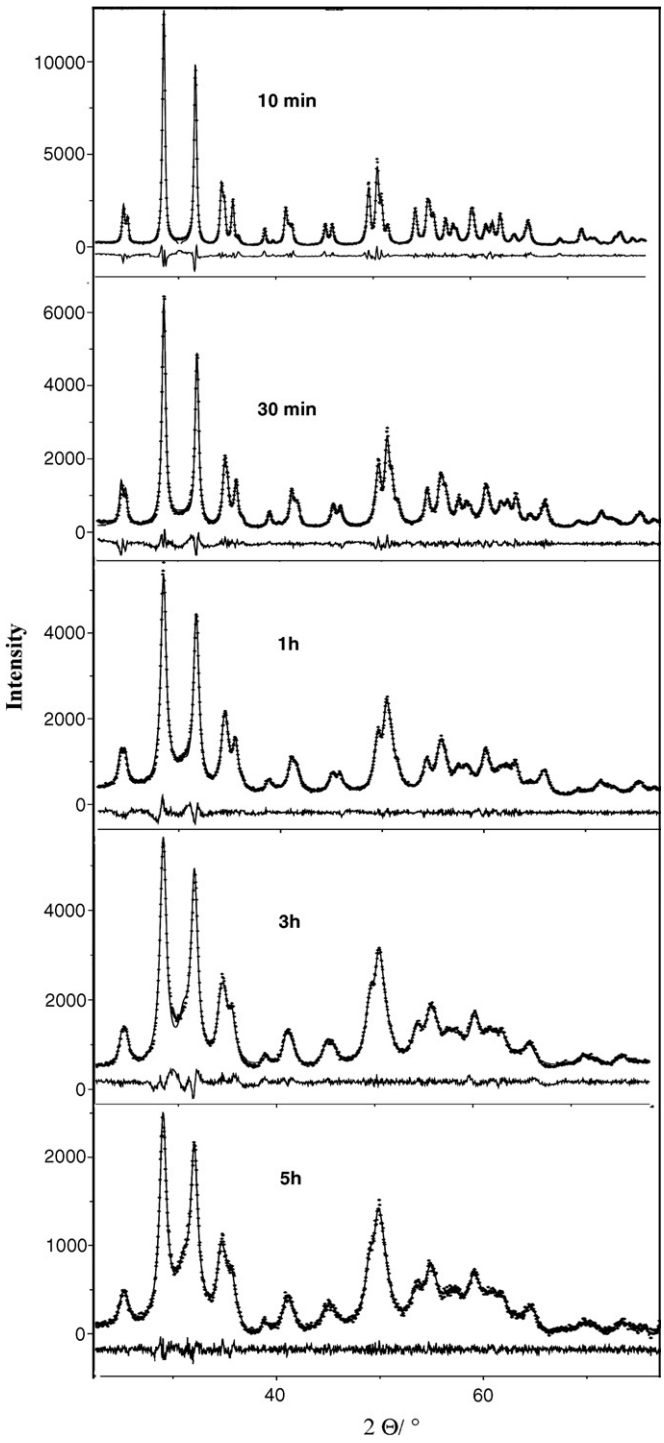

Fig. 1. The results of whole-powder-pattern profile refinements (program GSAS) of the products obtained by ball-milling with agate assembly. Milling time is denoted above patterns. The observed intensity data are plotted in the upper field as ♦, the calculated pattern is shown as a line in the same field, and the difference between the observed and calculated patterns is shown as a line in the lower field.

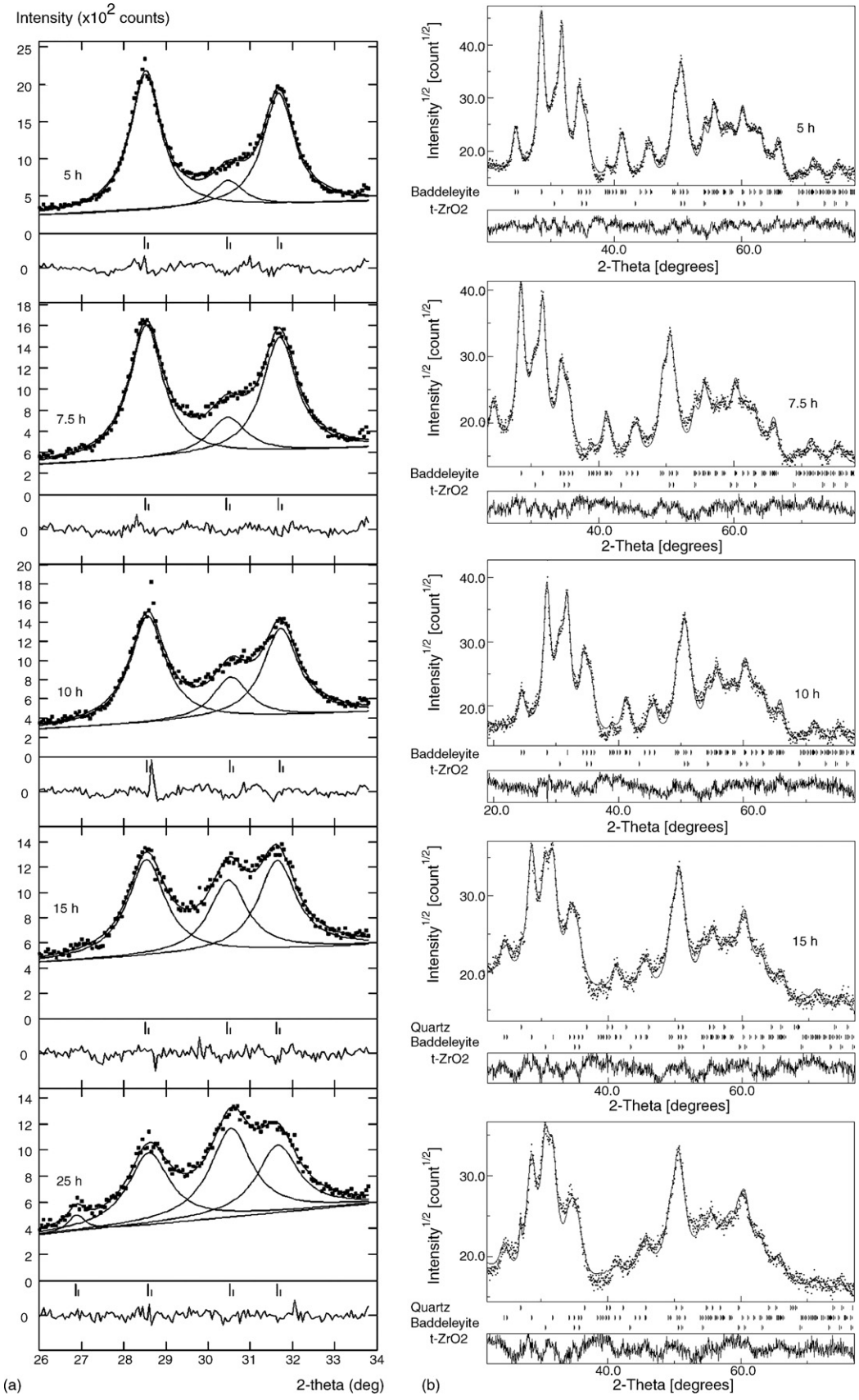

Fig. 2. The results of (a) individual profile fitting of the *m*-ZrO_2 diffraction lines ($\bar{1}11$) and (1 1 1) and the *t*-ZrO_2 diffraction line (1 0 1), (program PRO-FIT) and (b) quantitative Rietveld crystal phase analysis (program MAUD) of the products obtained by ball-milling with agate assembly. Milling time is denoted above patterns. The differences between the observed and refined patterns are shown in the box below.

Table 1
Values of the volume-averaged domain size D_v, and upper limits of micro-strain e, of m-ZrO_2 products calculated from the results of whole-powder-pattern profile refinements, and the corresponding values of weighted residual error (R_{wp} index)

Milling time	Corundum			Agate			Stainless steel		
	D_v/nm	$e \times 10^3$	R_{wp}	D_v/nm	$e \times 10^3$	R_{wp}	D_v/nm	$e \times 10^3$	R_{wp}
0 min	–	0.90	0.085	–	0.90	0.085	–	0.90	0.085
10 min	23	1.3	0.072	35.2	1.0	0.072	65	4.3	0.077
20 min	18.1	1.9	0.046	–	–	–	51	4.9	0.072
30 min	–	–	–	24.4	3.3	0.072	–	–	–
40 min	13.2	2.1	0.044	–	–	–	37	6.8	0.065
1 h	10.5	3.1	0.052	13.5	3.6	0.043	–	–	–
80 min	–	–	–	–	–	–	17.8	7.2	0.067
100 min	8.1	3.9	0.041	–	–	–	–	–	–
2 h	–	–	–	12.6	4.0	0.049	–	–	–
3 h	7.5	4.3	0.048	10.8	4.7	0.048	–	–	–
4 h	–	–	–	–	–	–	13.2	8.8	0.061
5 h	5.8	6	0.051	10.3	5.5	0.043	13.3	8.9	0.055
6 h	–	–	–	–	–	–	13.8	8.2	0.062
7 h	–	–	–	–	–	–	13.1	7.6	0.056
7.5 h	5.3	6.9	0.056	9.3	6.4	0.052	–	–	–
10 h	3.1	8.1	0.043	8.7	7.6	0.051	12.5	6.7	0.057
15 h	2.7	13.2	0.058	8.9	9.0	0.045	9.6[a]	6.0[a]	0.058
20 h	–	–	–	9.5	9.5	0.046	8.4[a]	9.9[a]	0.085
25 h	–	–	–	–	–	–	7.9[a]	8.8[a]	0.084
30 h	–	–	–	8.6	10.1	0.039	7.4[a]	9.7[a]	0.094
40 h	–	–	–	9.0	10.1	0.041	–	–	–

[a] Values obtained for t- or c-ZrO_2 products.

$$\Gamma_L = \frac{(X + Xe\cos\phi)}{\cos\theta} + (Y + Ye\cos\phi)\tan\theta + Z \quad (2)$$

where Γ is the full width at half maximum (FWHM) of the line profile, U, V, W, X, Y, Z, Xe and Ye are refinable parameters. The size and strain contribution to the line broadening can be given by the following equation:

$$\beta_S = \frac{\lambda}{(D_V\cos\theta)} \quad (3)$$

$$\beta_D = e\,4\tan\theta \quad (4)$$

where λ is the wavelength, D_v the volume-averaged domain size, e represents the upper limits of strain, while β_S and β_D represent the integral breadths of the Voigt function resulting from size and strain contribution, respectively. By comparing the Eqs. (1) and (2) with Eqs. (3) and (4) it is easy to recognize that parameters X, Xe and P will relate to size broadening and Y, Ye and U to strain broadening. Therefore, only these six parameters were refined in the line-broadening analysis of the ball-milling products. All other parameters assumed the values obtained upon the refinement of the standard (α-Si). In order to obtain pure physically broadened profile parameters, used in the calculation of β_S and β_D values, the obtained values of refined parameters U, X, Y, P for samples must be corrected by the corresponding values obtained for the standard. The results of the line broadening analysis are summarized in Table 1.

Precise determination of unit-cell parameters were performed using whole-powder-pattern refinements with two different methods, combined Le Bail method (program GSAS) and Pawley method[27] (program WPPF[28]). The fitting with the program WPPF was performed using the split-type pseudo-Voigt profile

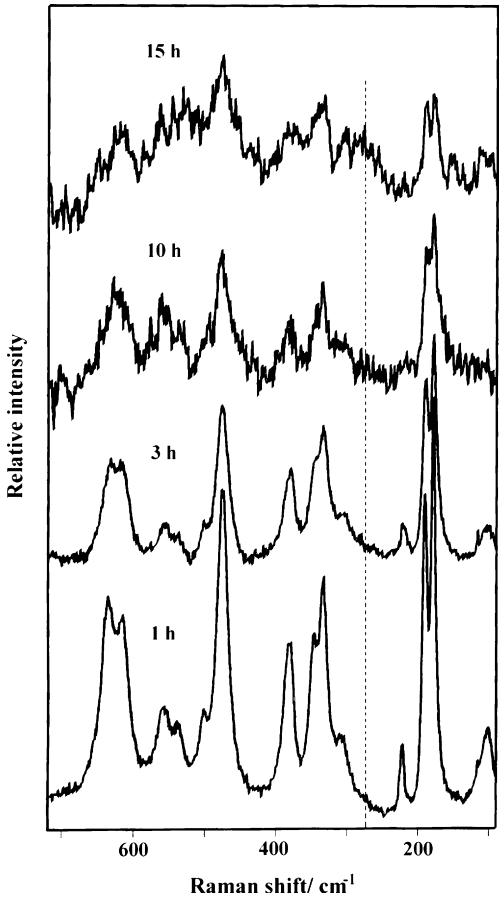

Fig. 3. Raman spectra of the products obtained by ball-milling with agate assembly. Milling time is denoted above spectra. Dotted line marks the position of the most prominent band typical of t-ZrO_2.

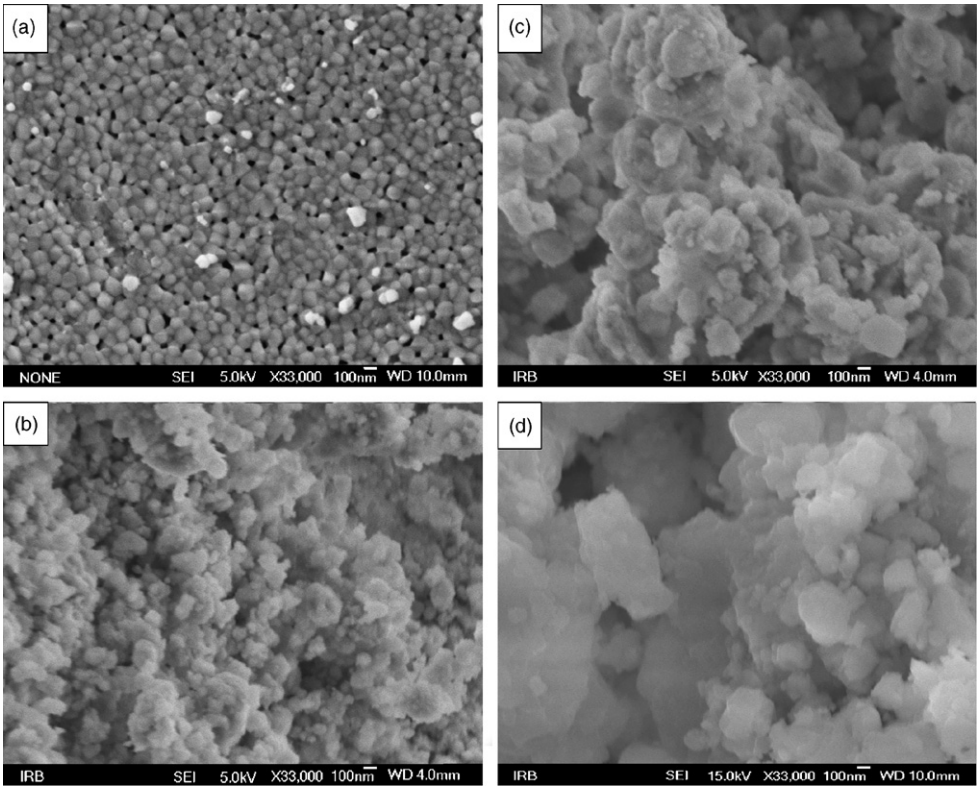

Fig. 4. FE SEM micrographs of ZrO_2 samples milled with agate milling assembly for (a) 0 h, (b) 3 h, (c) 15 h and 30 h.

Table 2
Volume fraction ratio $v_m/(v_m + v_t)$ of *m*-ZrO_2 and *t*-ZrO_2 and volume fraction of crystalline impurities, v_i (impurities = α-Al_2O_3, α-SiO_2 and α-Fe) estimated from the results of Rietveld refinement (program MAUD) and the corresponding ratio $v_m/(v_m + v_t)$ estimated from the results of individual profile fitting by following the procedure proposed by Toraya[31]

Milling assembly	Milling time	Rietveld refinement			Individual profile fitting	
		$\frac{v_m}{v_m+v_t}$	v_i	R_{wp}	$\frac{v_m}{v_m+v_t}$	R_{wp}
Corundum	3 h	0.90	0.32	0.078	0.93	0.043
	5 h	0.87	0.54	0.056	0.88	0.037
	7.5 h	0.83	0.73	0.074	0.80	0.038
	10 h	0.77	0.75	0.052	0.78	0.028
	15 h	0.77	0.75	0.065	0.76	0.047
	20 h	0.76	0.76	0.068	0.75	0.032
Agate	5 h	0.86	–	0.070	0.93	0.055
	7.5 h	0.84	–	0.069	0.90	0.046
	10 h	0.79	0.01	0.075	0.86	0.053
	15 h	0.76	0.02	0.072	0.77	0.038
	20 h	0.75	0.05	0.072	0.71	0.038
	25 h	0.71	0.08	0.073	0.67	0.044
	30 h	0.72	0.10	0.078	0.67	0.048
	40 h	0.73	0.12	0.072	0.66	0.035
	50 h	0.72	0.20	0.061	0.65	0.021
	70 h	0.77	0.23	0.067	0.70	0.028
Stainless steel	150 min	0.90	–	0.073	0.90	0.045
	4 h	0.90	–	0.074	0.89	0.054
	5 h	0.86	–	0.059	0.88	0.043
	7 h	0.86	0.01	0.079	0.88	0.051
	10 h	0.78	0.01	0.076	0.80	0.043
	15 h	0.41	0.04	0.078	0.42	0.041
	20 h	0	0.03	0.079	0	0.045
	25 h	0	0.02	0.067	0	0.051
	30 h	0	0.01	0.073	0	0.059
	30 h*	0.75	–	0.096	0.74	0.067

* Mixture of ZrO_2 sample milled for 30 h with stainless steel assembly and starting *m*-ZrO_2 sample (50 wt.%)

function and the polynomial background model. XRD patterns of the samples with added α-Si as an internal standard were collected in 2θ range from 20° to 100° with step 0.02, and counting time of 10 s per step.

Where monoclinic and tetragonal polymorphs of zirconia coexisted, the quantitative crystal phase analysis was performed using Rietveld refinements[29] of the powder diffraction patterns (program MAUD[30]). During the refinements we used fixed values for the crystallite size and lattice micro-strains obtained from the results of line-broadening analysis. The obtained values of the *t*-ZrO_2 and *m*-ZrO_2 volume fractions (v_t and v_m) were compared with the values obtained from the integral intensities of the monoclinic diffraction lines ($\bar{1}11$) and (1 1 1) and the tetragonal diffraction line (1 0 1), following a procedure proposed by Toraya et al.[31] The volume fractions are given by the following equations:

$$x = \frac{I_m(\bar{1}11) + I_m(111)}{I_m(\bar{1}11) + I_m(111) + I_t(101)} \quad (5)$$

$$v_t = 1 - v_m \quad (6)$$

$$v_m = \frac{1.311x}{1 + 0.311x} \quad (7)$$

Integrated intensities of the diffraction lines were determined using the individual profile-fitting method (computer program PRO-FIT[28]).

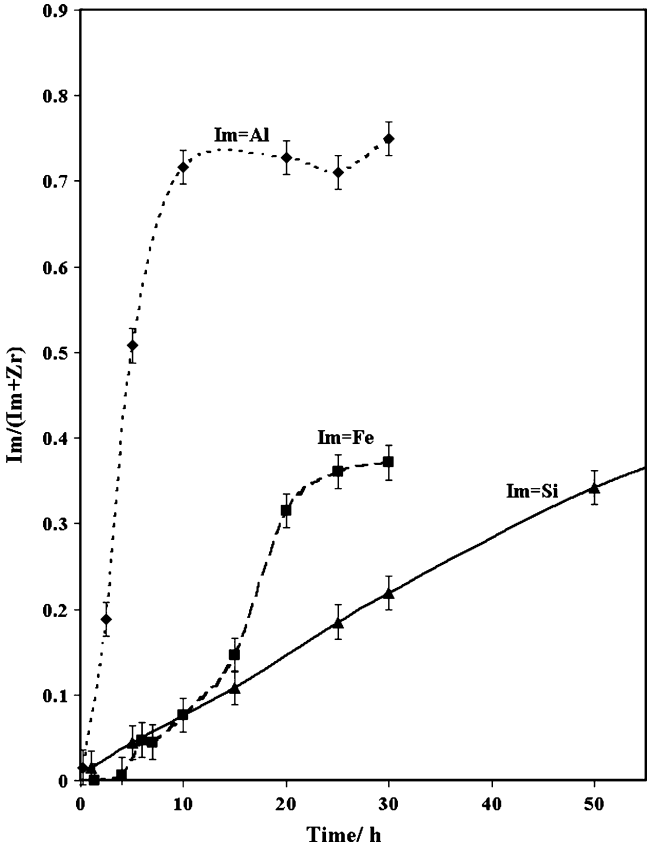

Fig. 5. The influence of milling time on the ratio between the amount of impurities (Im = Si, Al or Fe) and zirconium (Zr).

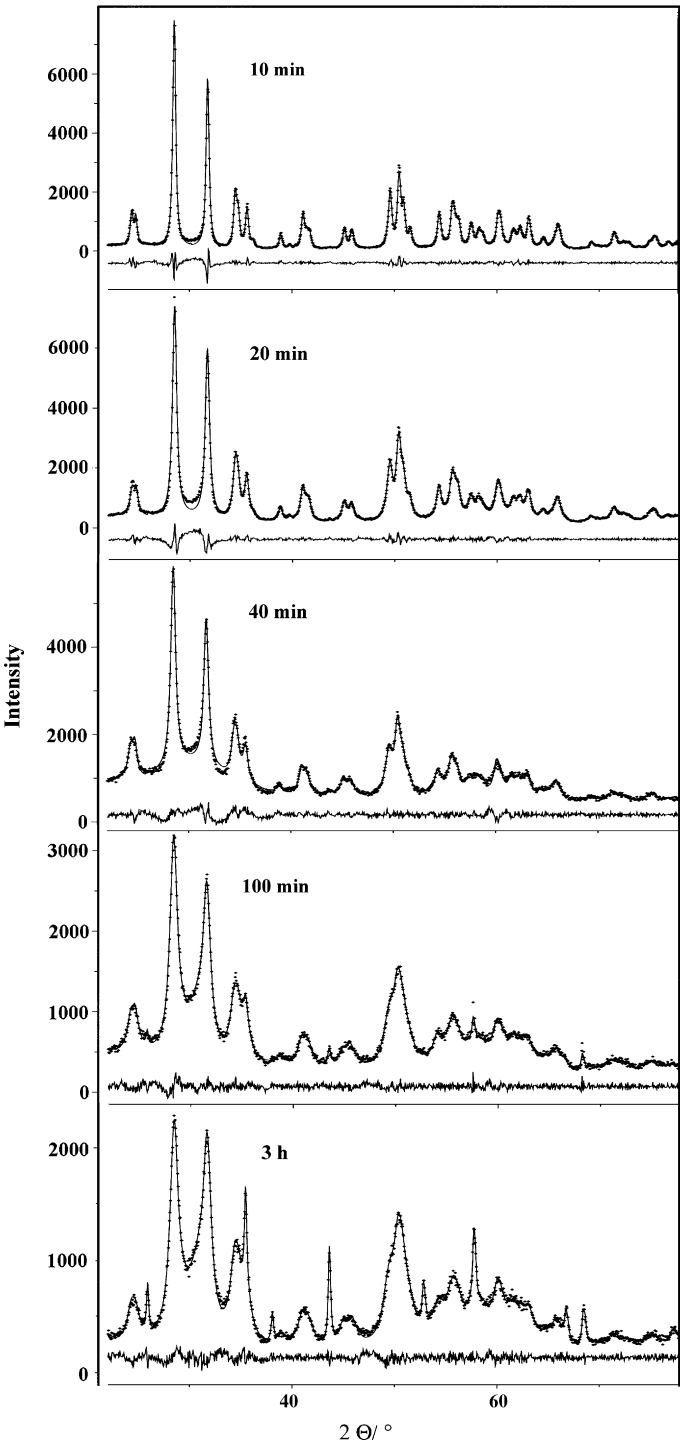

Fig. 6. The results of whole-powder-pattern profile refinements (program GSAS) of the products obtained by ball-milling with corundum assembly. Milling time is denoted above patterns. The observed intensity data are plotted in the upper field as ♦, the calculated pattern is shown as a line in the same field, and the difference between the observed and calculated patterns is shown as a line in the lower field.

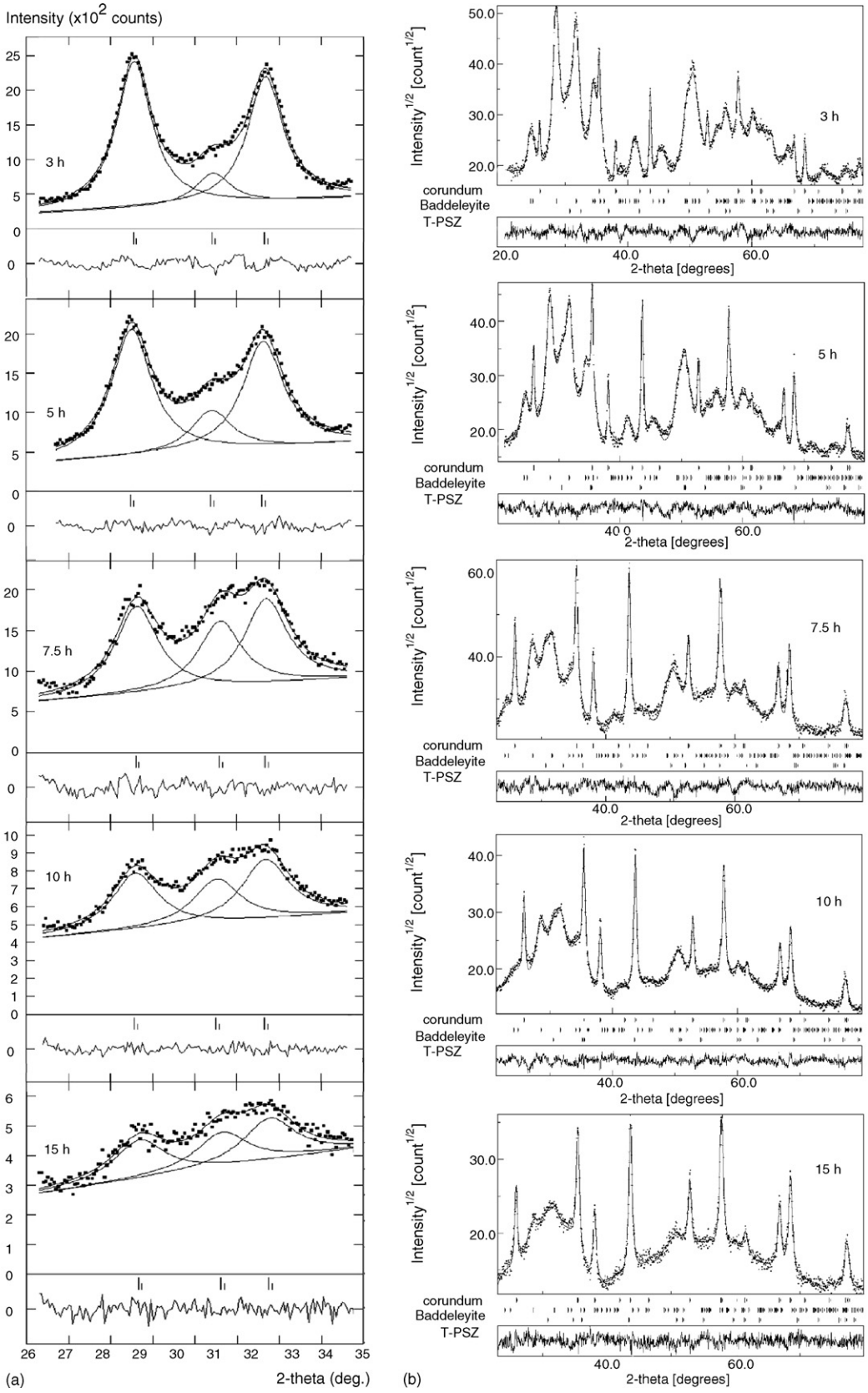

Fig. 7. The results of (a) individual profile fitting of the *m*-ZrO_2 diffraction lines ($\bar{1}11$) and (1 1 1) and the *t*-ZrO_2 diffraction line (1 0 1), (program PRO-FIT) and (b) quantitative Rietveld crystal phase analysis (program MAUD) of the products obtained by ball-milling with agate assembly. Milling time is denoted above patterns. The differences between the observed and refined patterns are shown in the box below.

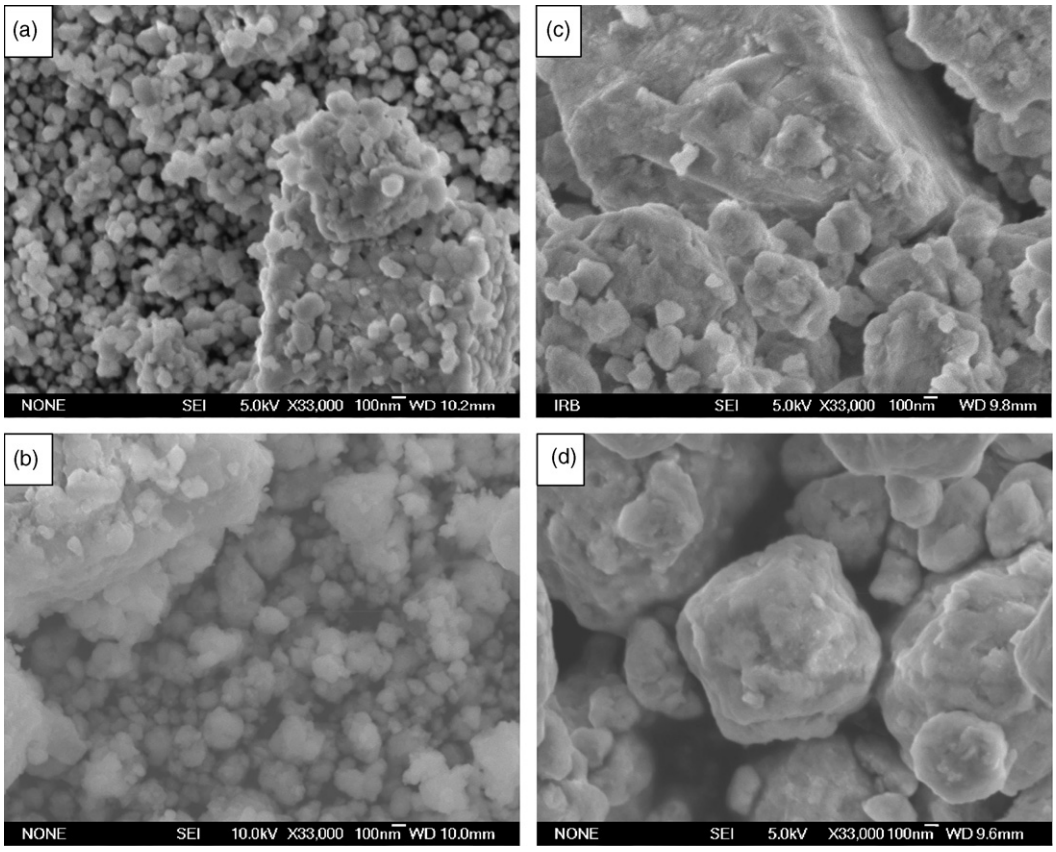

Fig. 8. FE SEM micrographs of ZrO_2 samples obtained by ball-milling with corundum assembly for (a) 10 min, (b) 150 min, (c) 10 h, and (d) 30 h.

4. Results

4.1. Agate milling assembly

The diffraction patterns of the starting materials contain only the very narrow diffraction lines typical of *m*-ZrO_2. The process of ball-milling causes significant broadening of these diffraction lines followed by the decrease of their intensities. The results of whole-powder-pattern profile refinements (Fig. 1) indicate a very small anisotropic size and strain broadening (the refined values of the parameters *X*e and *Y*e are nearly 0), which can be attributed to the fact that the *m*-ZrO_2 lattice represents just a minor distortion of the cubic fluorite structure. The spherical morphology of the crystallites in the starting and ball-milled samples justifies the isotropic model of line broadening. For this reason and in order to reduce the number of variables, only parameters *X* and *Y* were refined and used to estimate volume-averaged domain size, D_v, and upper limits of microstrain, *e*, of *m*-ZrO_2 crystallites. Small differences between the observed and calculated patterns and very low values of the R_{wp} (weighted residual error) index indicate a relatively good reliability of the extracted values (Fig. 1). The estimated values for D_v

Table 3
Refined values of unit-cell parameters of the *t*-ZrO_2 product obtained after ball-milling of initial *m*-ZrO_2 between 15 and 30 h

Time (h)	Lattice parameters of *t*-ZrO_2 products							
	GSAS program				WPPF program			
	a (Å)	*c* (Å)	*V* (Å^3)	R_{wp}	*a* (Å)	*c* (Å)	*V* (Å^3)	R_{wp}
15	3.5937(8)	5.1393(14)	66.4	0.058	3.585(3)	5.118(3)	65.8	0.104
	5.0822(11)[a]		132.8[a]		5.070(4)[a]		131.6[a]	
20	3.581(1)	5.081(3)	65.12	0.087	3.587(1)	5.064(2)	65.15	0.086
	5.0643(1)[a]		130.3[a]		5.071(2)[a]		130.3[a]	
25	3.565(1)	5.067(3)	64.4	0.096	3.564(1)	5.051(1)	64.2	0.091
	5.0418(1)[a]		128.8[a]		5.040(2)[a]		128.3[a]	
30	3.558(2)	5.051(4)	64.0	0.097	3.556(1)	5.045(2)	63.8	0.092
	5.035(3)[a]		128.0[a]		5.030(2)[a]		127.6[a]	

[a] Related to fluorite type lattice.

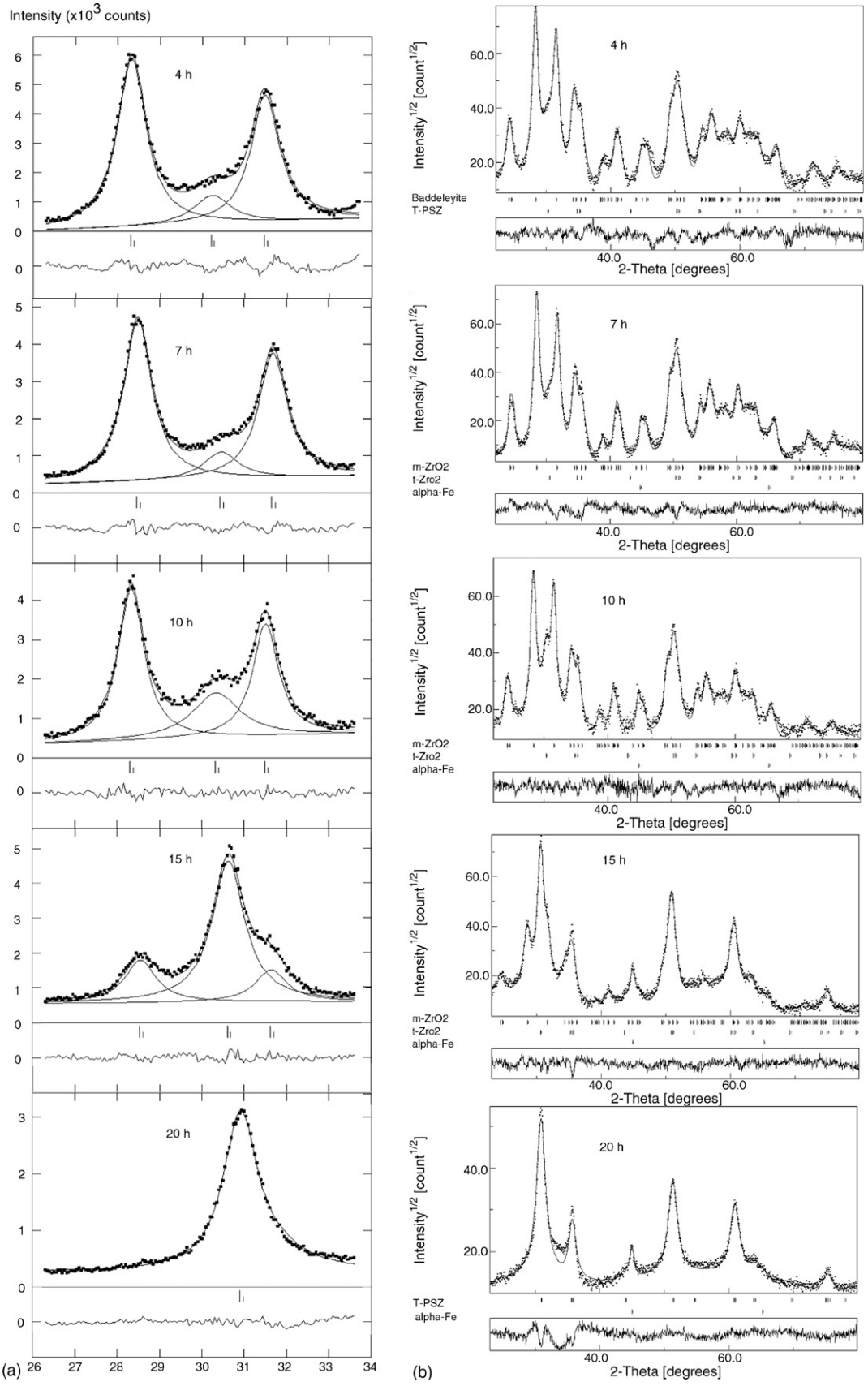

Fig. 9. The results of (a) individual profile fitting of the *m*-ZrO_2 diffraction lines ($\bar{1}11$) and (1 1 1) and the *t*-ZrO_2 diffraction line (1 0 1), (program PRO-FIT) and (b) quantitative Rietveld crystal phase analysis (program MAUD) of the products obtained by ball-milling with stainless steel assembly. Milling time is denoted above patterns. The differences between the observed and refined patterns are shown in the box below.

and e and the corresponding values of the R_{wp} index are given in Table 1. Onset of crystallite size decrease and micro-strain increase occurred in the first 2 h of ball-milling. Further milling causes a small decrease of D_v and increase of e values up to ~9 and ~0.010 nm, respectively (Table 1). XRD pattern of products milled for 5 h or more contain, beside the diffraction lines of m-ZrO_2, diffraction lines typical of t- or c-ZrO_2 (Fig. 2). The appearance of the shoulder on the lower angle side of the diffraction line 111 of m-ZrO_2 in XRD pattern of the product milled for 5 h indicates the appearance of the most prominent line typical of t- or c-ZrO_2. With a further increase of milling time this line become clearly visible. The presence of the band at ~270 cm^{-1} in the Raman spectrum of the corresponding milling products (Fig. 3) indicates that t-ZrO_2 is the product of phase transition. The results of quantitative crystal phase analysis (Table 2) show that partial-phase transition into t-ZrO_2 reached maximum after ~20 h of milling. Further milling had very small influence on the m-$ZrO_2 \rightarrow t$-ZrO_2 transition, so that m-ZrO_2 remained the dominant phase in all milled products. The first sign of the diffraction line typical of α-SiO_2 appeared in the product milled for 7.5 h. The intensity of α-SiO_2 diffraction lines increased with the increase of milling time due to wearing of the milling medium. However, the amount of α-SiO_2 phase remained relatively small even after a prolonged time of ball-milling (Table 2). The result of FE SEM analysis shows that starting m-ZrO_2 contains spherical mono-dispersed particles of ~100 nm in size (Fig. 4). The process of ball-milling caused a decrease of the particles to nano-dimensions covering a broad interval of diameters. Significant agglomeration of the nanometric particles prevents clear determination of the size distributions (Fig. 4). The results of EDS analysis show the appearance of Si contamination in the product ball-milled for 30 min. The amount of contamination increased almost linearly with an increase of milling time. However, even after a prolonged time of ball-milling (50 h) the amount of Si contamination remained relatively small (Fig. 5).

4.2. Corundum milling assembly

As in the case of the agate milling assembly the results of whole-powder-pattern profile refinements indicate isotropic size and strain broadening of the milling products (Fig. 6). The decrease of D_v values and increase of e values of m-ZrO_2 crystallites during the ball-milling occurred with a significantly higher rate compared to agate milling assembly and lead to almost complete amorphization after ~15 h of milling (Table 1). XRD patterns of the products ball-milled for 3 h or more contain, beside diffraction lines of m-ZrO_2, small and broad diffraction lines typical of t- or c-ZrO_2 and narrow diffraction lines typical of α-Al_2O_3 (Fig. 7). The results of quantitative crystal phase analysis (Table 2) indicate that α-Al_2O_3, introduced as a result of the wearing of milling media, become dominant crystal phase after 5 h of ball-milling. Significant contamination of the samples was also confirmed by the results of EDS analysis (Fig. 5). Raman spectra of products obtained after shorter milling times (up to 1 h) contain m-ZrO_2 bands which decrease in relative intensity and become broader with the increase of milling time. In Raman spectra of the products obtained after more than 1 h of milling the broad florescence background overlapped the Raman bands. The fluorescence background appeared in those spectra due to a considerable amount of corundum impurities introduced by wearing of the milling media. The results of FE SEM/EDS analysis (Fig. 8) show that the milling process caused a decrease of starting m-ZrO_2 particles, which after a prolonged milling time form agglomerates with significant amount of corundum impurities.

4.3. Stainless steel milling assembly

The results of whole-powder-pattern profile refinements show that after ~3 h of ball-milling the D_v values of m-ZrO_2 crystallites decreased to ~13 nm, whereas the e values increased to $\sim 8 \times 10^{-3}$ (Table 1). A further increase in the milling time up to 10 h had little impact on the D_v and e values. A very small amount of t- or c-ZrO_2 phase appeared in that early stage of ball-milling. The onset of the phase transition occurred after ~15 h of ball-milling and resulted in a complete transition into the high-temperature polymorph of ZrO_2 after 20 h of ball-milling (Fig. 9). The results of quantitative crystal phase analysis are summarized in Table 2. Raman spectra of the corresponding products show that the process of ball-milling cause a broad-

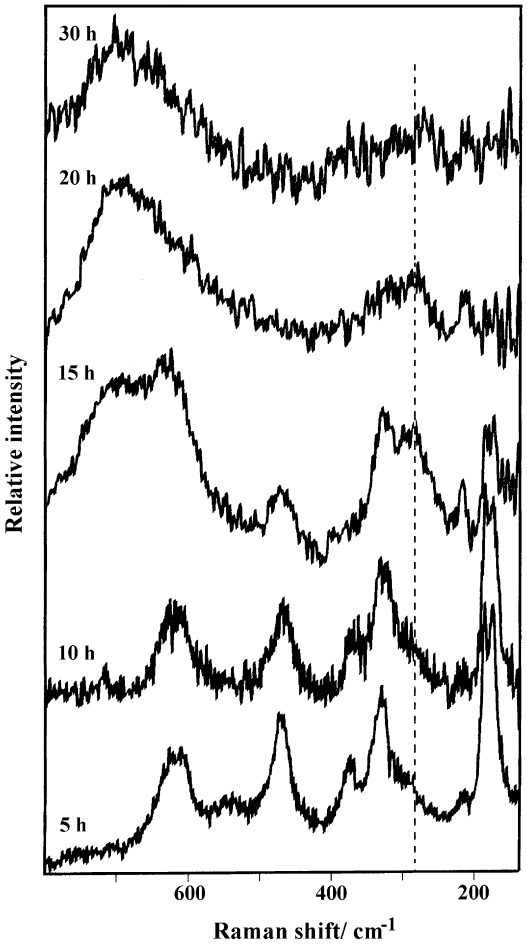

Fig. 10. Raman spectra of the products obtained by ball-milling with stainless steel assembly. Milling time is denoted above spectra. Dotted line marks the position of the most prominent band typical of t-ZrO_2.

ening and decrease of the bands typical of m-ZrO_2 and the appearance of the most prominent band typical of t-ZrO_2 at ∼270 cm^{-1} (Fig. 10). The bands typical of t-ZrO_2 become dominant in the Raman spectrum of the product ball-milled for 15 h. After 20 h of ball-milling, m-ZrO_2 bands disappeared, while the most prominent band typical of t-ZrO_2 could still be observed. With further ball-milling the bands typical of t-ZrO_2 almost completely disappeared, thus indicating a possible further transition to c-ZrO_2 (Fig. 10). In addition to the bands typical of ZrO_2, Raman spectra of the products ball-milled between 15 and 30 h also contain unidentified bands at ∼700 and 216 cm^{-1} (Fig. 10).

The volume-averaged domain size of the obtained t-ZrO_2 phase (15 h of ball-milling) was estimated to ∼10 nm (Table 1). Further ball-milling up to 30 h caused a small decrease of D_v values (∼8 nm) and increase in the e values (∼0.01). Beside the diffraction lines of ZrO_2 phases, XRD patterns of products ball-milled between 10 and 30 h contain the diffraction lines typical of α-Fe. The diffraction lines of α-Fe reached a maximum after 15 h of ball-milling. Further ball-milling caused a decrease in the diffraction lines of this phase, which almost disappeared after 30 h of ball-milling. The position of the diffraction lines in the t- or c-ZrO_2 phase shifted to a higher angle with the increased ball-milling time, indicating a decrease in the lattice parameters. The

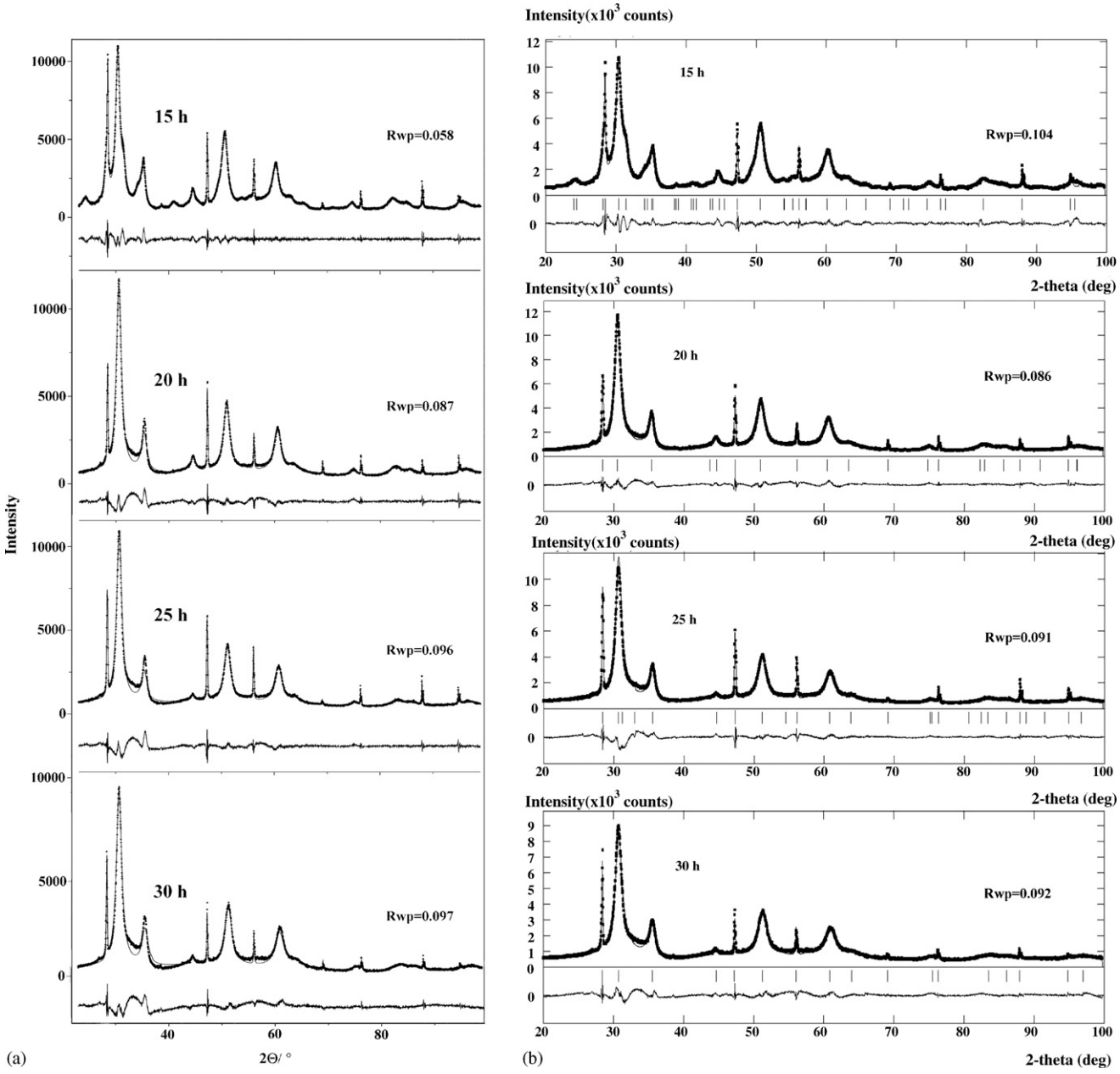

Fig. 11. Whole-powder-pattern decomposition results of the products milled between 15 and 30 h with stainless steel assembly and α-Si as internal standard, obtained using (a) Le Bail method (program GSAS) or (b) Pawley method (program WPPF). The difference between the observed and calculated patterns is shown as a line in the lower field.

results of the precise determination of lattice parameters of the products ball-milled from 15 to 30 h (Fig. 11) are summarized in Table 3. In these refinements we have assumed a tetragonal symmetry of ZrO_2 products.

The results of FE SEM analysis (Fig. 12) indicate gradual decrease of particles which kept a spherical morphology. The rate of the decrease appeared to be slower compared with agate and corundum milling assemblies. However, after prolonged milling time (20 h or more) most of the crystallites decreased to nanometric sizes and formed agglomerates (Fig. 12). The results of EDS analysis (Fig. 5) indicate very small amount of iron contamination in the early stage of ball-milling (up to ∼150 min). Stainless steel particles introduced during the ball-milling up to 10 h can be easily separated from the ZrO_2 particles. The onset of iron contamination occurred after about 15 to 20 h of milling (Fig. 5). However, regardless of a significant increase in the amount of iron, steel particles could not be detected. The estimated amount of impurities appeared to be almost the same at low and high magnifications and the results of element mapping, even at very high magnifications, indicated a uniform distribution of the impurities in all parts of the samples.

A comparison of the Mössbauer spectra of the stainless-steel powder, obtained as a wearing product upon 20 min of ball-milling with no ZrO_2 powder, and the sample obtained upon 30 h of ball-milling shows that the process of ball-milling caused an almost complete oxidation of the stainless steel particles introduced into the sample. The spectrum of the stainless steel powder (Fig. 13) is characterized by one single line. This singlet almost completely disappeared from the spectrum of product ball-milled for 30 h (Fig. 13). This Mössbauer spectrum shows a superposition of two doublets, one typical of Fe^{3+} (66%) and the other typical of Fe^{2+} (33%). The quadrupole splitting of the Fe^{3+} component can be assigned to the formation of a solid solution inside ZrO_2 particles. The quadrupole splitting of the Fe^{2+} component cannot be assigned to some of the mixed metal oxides which could be formed during the ball-milling process (e.g. $FeCr_2O_4$, $NiFe_2O_4$ or similar). It is more likely that Fe^{2+} is also present in the form of a solid solution or in the amorphous phase. The formation of a FeO_{1-x} phase was excluded on the basis of the parameters given in Table 4.

Table 4
RT Mössbauer parameters for iron impurities formed as wearing product during the ball-milling process

Time	I.S. (mm s^{-1})	Q (mm s^{-1})	Γ (mm s^{-1})	Area (%)
20 min	−0.14		0.43	100
30 h	0.21	1.06	0.60	66.4
	0.82	2.18	0.71	33.6

Key: I.S.: isomer shift related to α-Fe; Q: quadrupole splitting; Γ = line-width.

The fraction of the amorphous phase in the final product, obtained after 30 h of ball-milling, was determine by perform-

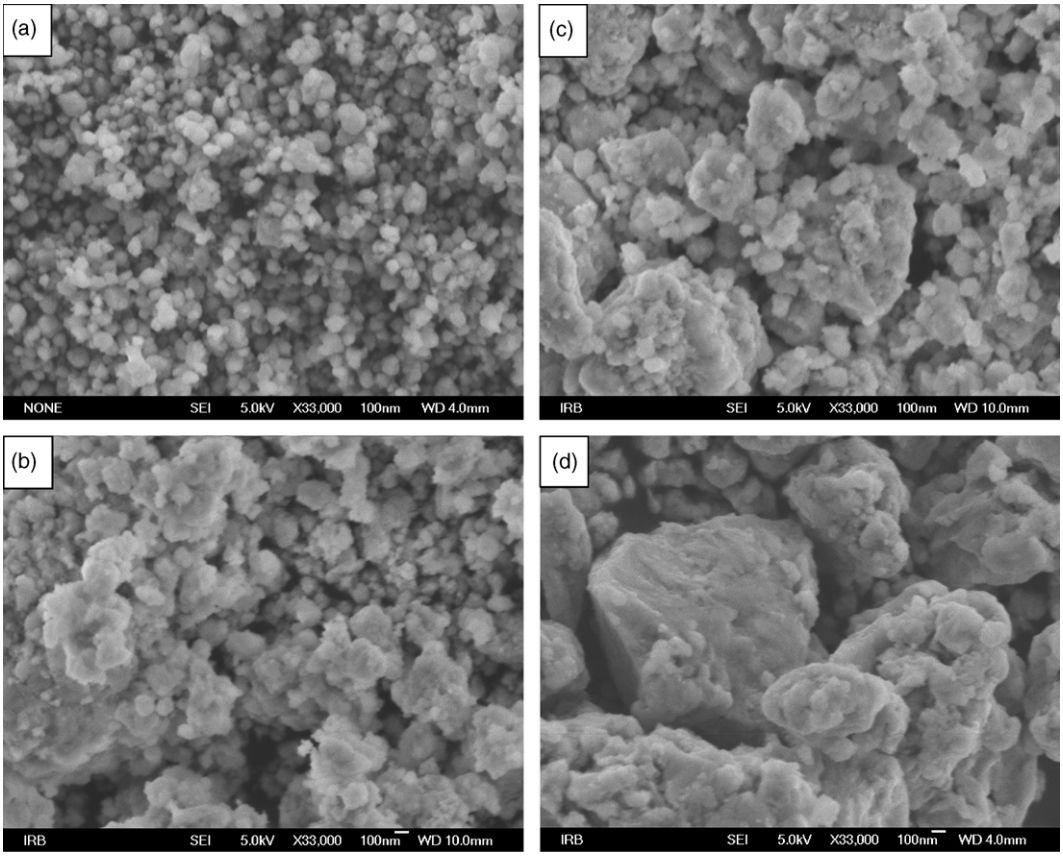

Fig. 12. FE SEM micrographs of ZrO_2 samples milled with stainless steel assembly for (a) 40 min, (b) 5 h, (c) 15 h, and (d) 30 h.

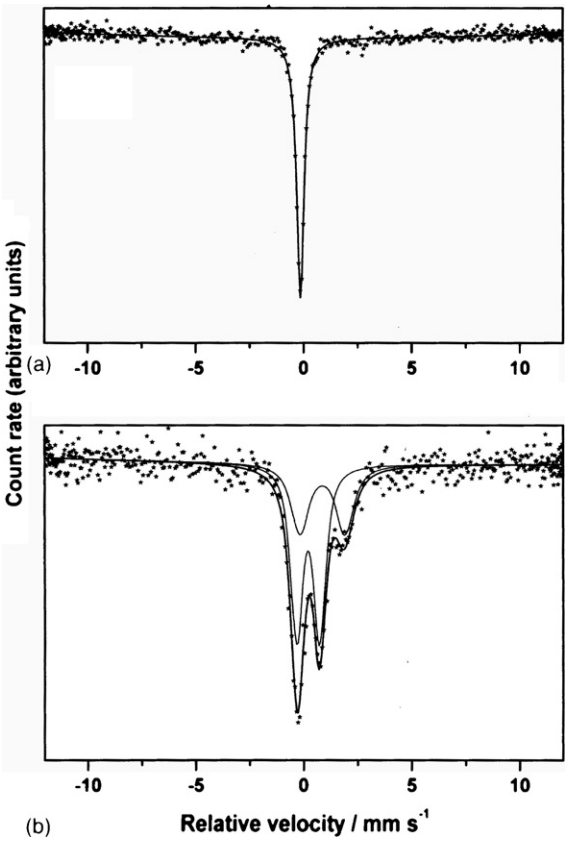

Fig. 13. RT Mössbauer spectra of (a) the stainless-steel powder and (b) the sample obtained upon 30 h of ball-milling.

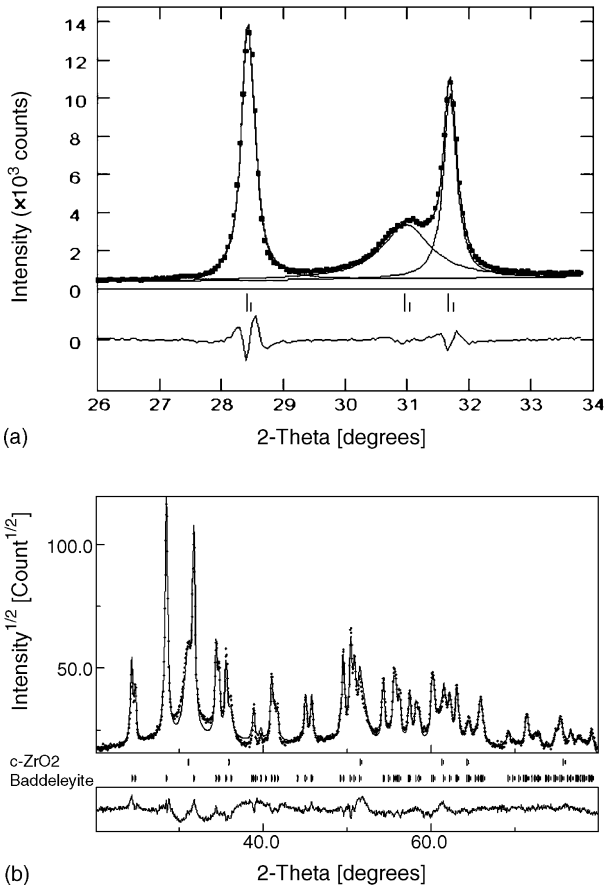

Fig. 14. The results of (a) individual profile fitting (program PRO-FIT) and (b) quantitative Rietveld crystal phase analysis (program MAUD) of the milled product (30 h with stainless steel assembly) with added m-ZO_2 (50 wt.%). The differences between the observed and refined patterns are shown in the box below.

ing quantitative crystal phase analysis after addition of a known amount of starting m-ZrO_2 (50 wt.%). Fig. 14 shows the results of Rietveld refinements and individual profile fitting of the obtained product. The result of these refinements (Table 2), after correction for small difference in the density between t-ZrO_2 and m-ZrO_2 phase, indicate that amorphous phase represents ∼60 wt% of the product ball-milled for 30 h.

5. Discussion

The first comparative study of the influence of milling medium (WC, corundum, stainless steel) on the structural and microstructural changes in m-ZrO_2 was given by Bailey et al.[9] The authors concluded that the differences in milling assemblies had very small influence on the phase development of m-ZrO_2. In all three cases partial m-$ZrO_2 \rightarrow t$-ZrO_2 transition resulted in the formation of m-$ZrO_2 + t$-ZrO_2 mixture with ∼45% of metastable phase.[9] In contrast to that, the results presented here show that the structural and microstructural developments of m-ZrO_2 during the ball-milling strongly depend on the type of milling assembly used. The results of line broadening analysis and quantitative crystal phase analysis of the milled products obtained using all three milling assembles are summarized in Fig. 15. The obtained results indicate that there is no clear connection between crystallite size decrease/micro-strain increase and m-$ZrO_2 \rightarrow t$-ZrO_2 transition. Regardless of the type of milling medium, the onset of crystallite size decrease and micro strain increase occurred in the early stage of ball-milling. On the other hand, the onset of m-$ZrO_2 \rightarrow t$-ZrO_2 transition occurs only in the product ball-milled with stainless steel milling assembly after ∼15 h of milling and results in the complete transition after 20 h. The appearance of the bands typical of t-ZrO_2[19–21] in the Raman spectra of the corresponding products (Fig. 10) clearly shows that the product of m-ZrO_2 transition is t-ZrO_2. A significant decrease and disappearance of t-ZrO_2 bands after ball-milling for 30 h indicated a probable further transition into c-ZrO_2 (Fig. 10). The results of XRD analysis appeared to be in accordance with the results of Raman spectroscopy. As a first step in determining precisely the unit-cell parameters of a t- or c-ZrO_2 product obtained after 15 h of ball-milling with stainless steel assembly, we have assumed cubic symmetry. The results obtained after refinement (program GSAS) indicate a considerably higher unit-cell parameter (0.5112 nm) than reported for c-ZrO_2 (0.5088 nm; ICDD PDF No. 27–0997). The same fact was observed by Bid and Pradhan[17] (the unit-cell parameter of c-ZrO_2 product was estimated to be >0.5125). After assuming tetragonal symmetry, the value of the R_{wp} index decreased and the obtained results indicated a considerable difference between

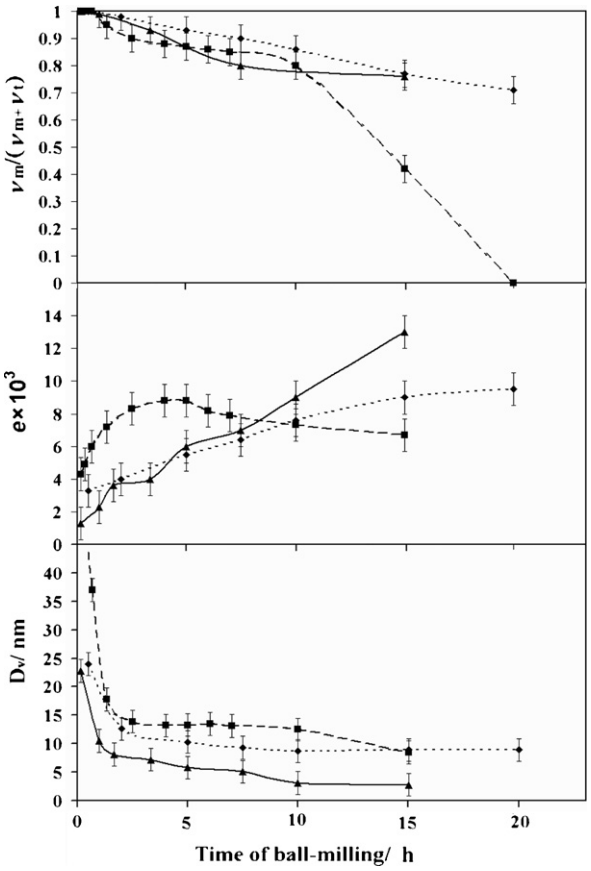

Fig. 15. Influence of milling time on the volume-averaged domain size (D_v), upper limits of micro-strain (e) and ratio between volume fraction of m-ZrO_2 and t-ZrO_2. Corundum (▲;); Agate (♦); stainless steel (■.)

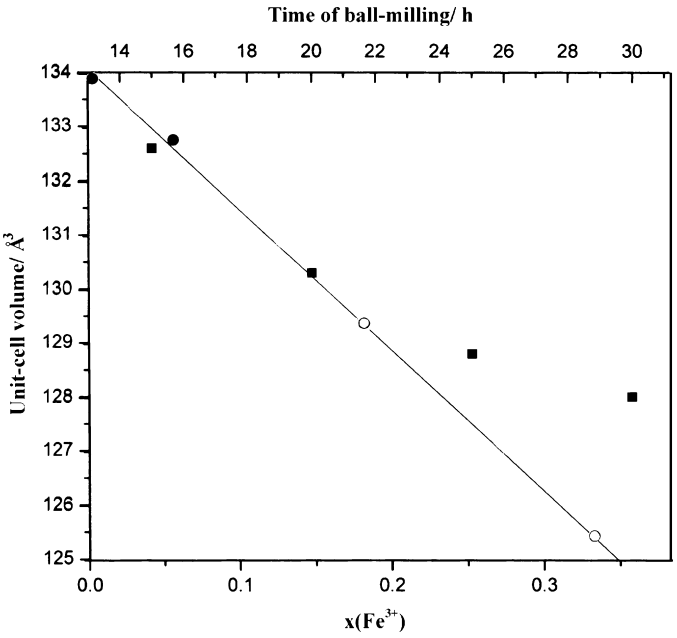

Fig. 16. Influence of molar fraction of Fe^{3+} ions (bottom abscissa) on the unit-cell volume of c-ZrO_2 (◯) and t-ZrO_2 (●) type solid solutions[42] and the corresponding influence of milling time (top abscissa) on the unit cell-volume of t- or c-ZrO_2 products (■).

c_f and a_f axes (Table 3). On the other hand, the axial ratio c_f/a_f of the products ball-milled between 20 and 30 h approached 1 (Table 3), indicating a transition toward c-ZrO_2.

Another objective of the present work was to determine the factor(s) which caused the observed transitions. The results of EDS analysis (Fig. 5) indicate a significant increase and homogeneous distribution of iron and chromium impurities during the period of ball-milling connected with the onset of m-$ZrO_2 \rightarrow t$-ZrO_2 transition. A uniform distribution of the impurities, determined from the results of element mapping, indicates possible incorporation into ZrO_2 particles. The incorporation of elemental iron or chromium is highly unlikely, but the incorporation of their cations (Fe^{2+}, Fe^{3+} or Cr^{3+}) is well known.[32,33] The results of precise lattice parameter measurements show a significant decrease in the lattice parameters of t- or c-ZrO_2 products with the increase of ball-milling time (Table 3). The same effect was observed by Bid and Pradhan.[17] Such a decrease can result from the incorporation of undersized dopants such as Fe^{3+} or Cr^{3+} ions.[32,33] The incorporation of aliovalent ions stabilizes the high-temperature polymorph of ZrO_2 by introducing oxygen vacancies and reducing the coordination number of Zr^{4+} ions.[8] Our previous investigation showed that the incorporation of Fe^{3+} ions into ZrO_2 lattice caused linear decrease of the unit-cell volume and stabilization of tetragonal (Fe^{3+} ions below 20 mol.%) or cubic polymorph of ZrO_2 (Fe^{3+} ions above 20 mol.%).[33] A comparison of the unit-cell volume of our ball-milled ZrO_2 products and the unit-cell volume resulting from the incorporation of Fe^{3+} ions (Fig. 16) indicate that the products milled for 25 or 30 h are in the range where stabilization of the cubic polymorph of ZrO_2 occurs.[33] The results of Mössbauer spectroscopy clearly show that the process of ball-milling caused an almost complete oxidation of iron present in the samples (Fig. 13). The incorporation of these aliovalent cations causes a stabilization of tetragonal and cubic polymorphs of ZrO_2 in the products ball-milled with stainless steel milling assembly.

In the case of the products ball-milled with corundum or agate milling assembly partial m-$ZrO_2 \rightarrow t$-ZrO_2 transition occurs, resulting in the formation of about 25–30% of metastable phase (Table 2). This partial transition could not be clearly connected with ZrO_2 crystallite size or the presence of impurities. The ball-milling with corundum milling assembly has the strongest impact on the decrease in size of crystallites and micro-strain increase, and causes almost complete amorphization of the starting m-ZrO_2. However, regardless of such a strong impact on the microstructure, the ball-milling with corundum milling assembly has the least impact on phase transition to metastable t-ZrO_2 (Table 2). A significant amount of Al_2O_3 impurities, introduced during the milling process (Fig. 5), also has little influence on the stabilization of t-ZrO_2. The reason for that can be attributed to the big difference between the radius of Al^{3+} and Zr^{4+} ions[34] which prevent significant incorporation of aliovalent cation into ZrO_2 lattice.[20] Similarly, the presence of SiO_2 in the product ball-milled with agate milling assembly does not have significant influence on the stabilization of t-ZrO_2. Partial m-$ZrO_2 \rightarrow t$-ZrO_2 transition observed in the product ball-milled with corundum and agate milling assembles can be attributed to

the combined contributions of lattice defects, impurities, crystallite size and the energy shared during the ball-milling process. It is well known that the process of ball-milling can cause partial formation of metastable phase in the case of products which undergoes martensitic transformation.[10] A significant share of energy during the process of ball-milling can cause partial transition of starting thermodynamically stable *m*-ZrO_2 to metastable phase. Upon a prolonged time of ball-milling the dynamic equilibrium occurs. The fraction of the metastable phase at the equilibrium will depend on the energy difference between metastable and thermodynamically stable phase (influence of particle size, lattice defects, impurities) and the energy shared during the process. The obtained results clearly show that the partial transition could not be attributed to a single effect such as the effect of crystallite size decrease.

6. Conclusions

The obtained results show that structural and microstructural developments of *m*-ZrO_2 during the ball-milling process strongly depend on the type of milling assembly used. Ball-milling with corundum milling assembly cause almost complete amorphization of the starting *m*-ZrO_2. The results of line broadening analysis indicated that ball-milling with agate or stainless steel assembly cause a decrease of the volume-averaged domain size to ∼9 nm or ∼13 nm, respectively. The results of Rietveld quantitative crystal phase analysis indicated that, regardless of the type of milling assembly, a small amount of tetragonal (*t*-)ZrO_2 appeared in the products ball-milled for 3 h or more. The onset of *m*-ZrO_2 → *t*-ZrO_2 transition occurred only in the products ball-milled with stainless steel assembly and resulted in a complete transition after 20 h of milling. Further ball-milling caused a decrease of the *t*-ZrO_2 lattice parameters followed by a probable transition into cubic (*c*-)ZrO_2. The stabilization of *t*- and c-ZrO_2 in a product milled with stainless steel assembly can be attribute to the incorporation of aliovalent cations (Fe^{2+}, Fe^{3+} or $Cr^{3+)}$ introduced into the sample due to the wear and oxidation of the milling media. The small fraction of metastable *t*-ZrO_2 formed in the product milled with corundum or agate milling assembly probably resulted from the combined contributions of lattice defects, impurities, crystallite size and the energy shared during the ball-milling process.

References

1. Garvie, R. C., The occurrence of metastable tetragonal zirconia as a crystallite size effect. *J. Phys. Chem.*, 1965, **69**, 1238–1243.
2. Garvie, R. C., Stabilization of the tetragonal structure in zirconia microcrystals. *J. Phys. Chem.*, 1978, **82**, 218–224.
3. Mitsuhasi, T., Ichihara, M. and Tatsuke, U., Characterization, and stabilization of metastable tetragonal ZrO_2. *J. Am. Ceram. Soc.*, 1974, **57**, 97–101.
4. Cypres, R., Wollast, R. and Raucq, J., Contribution on the polymorphic conversion of pure zirconia. *Ber. Dtsch. Keram. Ges.*, 1963, **40**, 527–532.
5. Livage, J., Doi, K. and Mazieres, C., Nature and thermal evolution of amorphous hydrated zirconium oxide. *J. Am. Ceram. Soc.*, 1968, **51**, 349–353.
6. Torralvo, J., Alario, M. A. and Soria, J., Crystallization behavior of zirconium oxide gels. *J. Catal.*, 1984, **86**, 473–476.
7. Štefanić, G., Gržeta, B., Popović, S. and Musić, S., In situ phase analysis of the thermal decomposition products of zirconium salts. *Croat. Chem. Acta*, 1999, **72**, 395–412.
8. Štefanić, G. and Musić, S., Factors influencing the stability of low temperature tetragonal ZrO_2. *Croat. Chem. Acta*, 2002, **75**, 727–767.
9. Bailey, E., Lewis, D., Librant, Z. M. and Porter, L. J., Phase transformations in milled zirconia. *Trans. J. Br. Ceram. Soc.*, 1972, **71**, 25–30.
10. Suryanarayana, C., Mechanical alloying and milling. *Prog. Mater. Sci.*, 2001, **46**, 1–184.
11. Chadwick, AV, Pooley MJ, Rammutla, KE, Savin, SLP, Rougier, A, A comparison of the extended x-ray absorption fine structure of nanocrystalline ZrO_2 prepared by high-energy ball milling and other methods. 2003,**15**, 431–440.
12. Chen, Y. L., Zhu, M., Qi, M., Yang, D. Z. and Fecht, H. J., *Mater. Sci. Forum*, 1995, **179–181**, 133.
13. Scian, A. N., Aglietti, E. F., Caracoche, M. C., Rivas, P. C., Pasquevich, A. F. and Garcia, A. R. L., Phase transformation in monoclinic zirconia caused by milling and subsequent annealing. *J Am. Ceram. Soc.*, 1994, **77**, 1525–1530.
14. Lin, J.-D. and Duh, J.-G., The use of X-ray line profile analysis in the tetragonal to monoclinic phase transformation of ball-milled, as sintered and thermally aged zirconia powders. *J. Mater. Sci.*, 1997, **32**, 4901–4908.
15. Murase, Y. and Kato, E., Phase transformation of zirconia by ball-milling. *J. Am. Ceram. Soc.*, 1979, **62**, 527.
16. Gajović, A., Furić, K., Štefanić, G. and Musić, S., In situ high temperature study of ZrO_2 ball-milled to nanometer sizes. *J. Mol. Struct.*, 2005, **744–747**, 127–133.
17. Bid, S. and Pradhan, S. K., Preparation and microstructure characterization of ball-milled ZrO_2 powder by the Rietveld method: monoclinic to cubic phase transformation without any additive. *J. Appl. Cryst.*, 2002, **35**, 517–525.
18. Liu, X., Wang, Z. and Bian, X., Monoclinic to cubic phase transformation of ZrO_2 induced by ball milling. *J. Mater. Sci.*, 2004, **39**, 2585–2587.
19. Yashima, M., Arashi, H., Kakihana and Yoshimura, M., Raman scattering study of cubic-tetragonal phase transition in $Zr_{1-x}Ce_xO_2$ solid solution. *J. Am. Ceram. Soc.*, 1994, **77**(4), 1067–1071.
20. Štefanić, G., Musić, S. and Trojko, R., The influence of thermal treatment on the phase development in HfO_2–Al_2O_3 and ZrO_2–Al_2O_3 systems. *J. Alloy. Compd.*, 2005, **388**, 126–137.
21. Merle, T., Guinebretiere, R., Mirgorodsky, A. and Quintard, P., Polarized Raman spectra of tetragonal pure ZrO_2 measured on epitaxial films. *Phys. Rev.*, 2002, **B 65**, 144302-1–1144302-6.
22. Powder Diffraction File, International Center for Diffraction Data, Newtown Square, Pa, 19073-3273, U.S.A.
23. Larson, AC, Von Dreele, RB, General structure analysis system GSAS. *Los Alamos National Laboratory Report* 2001.
24. Balzar, D., Audebrand, N., Daymond, M., Fitch, A., Hewat, A., Langford, J. I., Le Bail, A., Louër, D., Masson, O., McCowan, C. N., Popa, N. C., Stephens, P. W. and Toby, B., Size-strain line-broadening analysis of the ceria round-robin sample. *J. Appl. Cryst.*, 2004, **37**, 911–924.
25. Le Bail, A., Duroy, H. and Fourquet, J. L., Ab initio structure determination of $LiSbWO_6$ by X-ray powder diffraction. *Mater. Res. Bull.*, 1988, **23**, 447–452.
26. Thompson, P., Cox, D. E. and Hastings, J. B., Rietveld refinement of Debye–Scherrer synchrotron X-ray data from Al_2O_3. *J. Appl. Cryst.*, 1987, **20**, 79–83.
27. Pawley, G. S., Unit-cell refinement from powder diffraction scans. *J. Appl. Cryst.*, 1981, **14**, 357–361.
28. Toraya, H., Whole-powder-pattern fitting without reference to a structural model: application to X-ray powder diffractometer data. *J. Appl. Cryst.*, 1986, **19**, 440–447.
29. Rietveld, H. M., A profile refinement method for nuclear and magnetic structures. *J. Appl. Cryst.*, 1969, **2**, 65–71.
30. Lutterotti, L., Matthies, S. and Wenk, H.-R., MAUD (Material Analysis Using Diffraction): a user friendly Java program for Rietveld texture analysis and more. *Proceedings of the twelfth international conference on textures of materials (ICOTOM-12)*, 1999, **1**, 1599.

31. Toraya, H., Yoshimura, M. and Somiya, S., Calibration curve for quantitative analysis of the monoclinic-tetragonal ZrO_2 system by X-ray diffraction. *J. Am. Ceram. Soc.*, 1984, **67**, C119–C121.
32. Štefanić, G., Musić, S. and Gajović, A., Thermal behaviour of the amorphous precursors of the ZrO_2-CrO1.5 system. *J. Mol. Struct.*, 2005, **744–747**, 541–549.
33. Štefanić, G., Gržeta, B., Nomura, K., Trojko, R. and Musić, S., The influence of thermal treatment on the phase development in ZrO_2–Fe_2O_3 and HfO_2–Fe_2O_3 systems. *J. Alloy. Compd.*, 2001, **327**, 151–160.
34. Shannon, R. D., Revised effective ionic radii and systematic studies of interatomic distances in halides and chalcogenides. *Acta Crystallogr.*, 1976, **A 32**, 751–767.